Journal of Controlled Release 376 (2024) 402–412

Contents lists available at ScienceDirect

Journal of Controlled Release

journal homepage: www.elsevier.com/locate/jconrel

Injectable self-assembling peptide hydrogel as a promising vitreous substitute

Yuting Cai [a,1], Yatong Xiang [b,1], Huilei Dong [b,*], Wenjing Huang [b], Yan Liu [c], Chenguang Zhao [b], Dan Yuan [b], Yun Li [a,*], Junfeng Shi [b,d,*]

[a] Department of Ophthalmology, The Second Xiangya Hospital, Central South University, Changsha 410011, Hunan, PR China
[b] Hunan Provincial Key Laboratory of Animal Models and Molecular Medicine, State Key Laboratory of Chemo/Bio-Sensing and Chemometrics, School of Biomedical Sciences, Hunan University, Changsha 410082, Hunan, PR China
[c] Affiliated Hospital of Hunan University/Ophthalmology Department of Xiangtan Central Hospital, Hunan province, China
[d] Greater Bay Area Institute for Innovation, Hunan University, Guangzhou 511300, Guangdong, PR China

ARTICLE INFO

Keywords:
Peptide hydrogel
Self-assembly
Vitreous substitute
Biocompatibility
Optical coherence tomography

ABSTRACT

Vitreoretinal diseases pose significant threats to vision, often requiring vitrectomy and substitution of vitreous humor to restore ocular structure and visual function. However, existing substitutes have limitations that compromise patient outcomes. Supramolecular hydrogels, particularly peptide-based formulations, have emerged as promising alternatives due to their superior optical clarity, biocompatibility, and viscoelasticity. In this study, we designed and evaluated two peptide hydrogels, 3K-OX and 3E-OX, bearing positive and negative charges, respectively, as potential vitreous substitutes. Our in vitro findings revealed that the physicochemical properties of the negatively charged peptide hydrogel, 3E-OX, closely resembled those of the native vitreous body, exhibiting optimal light transmittance, refractive index, molecular permeability, and biocompatibility. Animal studies further confirmed the safety and biocompatibility of 3E-OX as a promising vitreous substitute. Notably, we introduced optical coherence tomography for retinal microvascular detection in non-pigmented rabbits, presenting a novel approach to evaluate the performance of intraocular tamponade materials. This work not only expands the utility of peptide hydrogels but also provides valuable insights into the design of vitreous substitutes.

1. Introduction

Vitreoretinal diseases pose a significant threat to vision health globally, affecting the life cycle, from infants to the elderly [1–4]. Among the treatments available, vitrectomy stands as the primary approach, involving the removal of the vitreous body and its replacement with substitutes to maintain ocular structure, facilitate retinal reattachment, and restore visual function. Ideally, these substitutes should closely mimic the structure and function of the human vitreous body [5–8]. However, current available vitreous substitutes bear notable shortcomings that greatly undermine patient outcomes [9]. For example, lactate Ringer's solution (LRS) lacks sufficient surface tension and tissue support for complex cases; gas tamponades (e.g. air, SF_6, C_3F_8, etc.) require patients an exhaustive face-down position, air travel restrictions, and cause an increased risk of cataracts, all of which compromise patients' quality of life [10]; Perfluorocarbon liquids are

Abbreviation: LRS, lactate Ringer's solution; SO, silicone oil; AM, Rink Amide; DIPEA, ethyldiisopropylamine; TFA, trifluoroacetic acid; GSSG, L-glutathione oxidized; RP-HPLC, reverse-phase high-performance liquid chromatography; CD, circular dichroism; 3D, three-dimensional; OCT, optical coherence tomography; OCTA, optical coherence tomography angiography; ERG, electroretinogram; DA, dark-adapted; LA, light-adapted; H&E, hematoxylin-eosin; SD, standard deviation; VAD, vessel area density; VDI, vessel diameter index; E, glutamic acid residues; K, lysine residues; BTP, bis-tris propane; PBS, phosphate buffered solution; TEM, transmission electron microscopy; ARPE19, adult retinal pigment epithelial cell line 19; NHDF, human dermal fibroblast; MIO-M1, Moorfields/Institute of Ophthalmology-Müller 1; IOP, intraocular pressure.

* Corresponding authors at: Hunan Provincial Key Laboratory of Animal Models and Molecular Medicine, State Key Laboratory of Chemo/Bio-Sensing and Chemometrics, School of Biomedical Sciences, Hunan University, Changsha 410082, Hunan, PR China; Department of Ophthalmology, The Second Xiangya Hospital, Central South University, Changsha 410011, Hunan, PR China.
E-mail addresses: huileidong@ncu.ecd.cn (H. Dong), yun.li@csu.edu.cn (Y. Li), jeff-shi@hnu.edu.cn (J. Shi).
[1] These authors contributed equally to this work.

https://doi.org/10.1016/j.jconrel.2024.10.016
Received 3 May 2024; Received in revised form 15 September 2024; Accepted 11 October 2024
Available online 21 October 2024

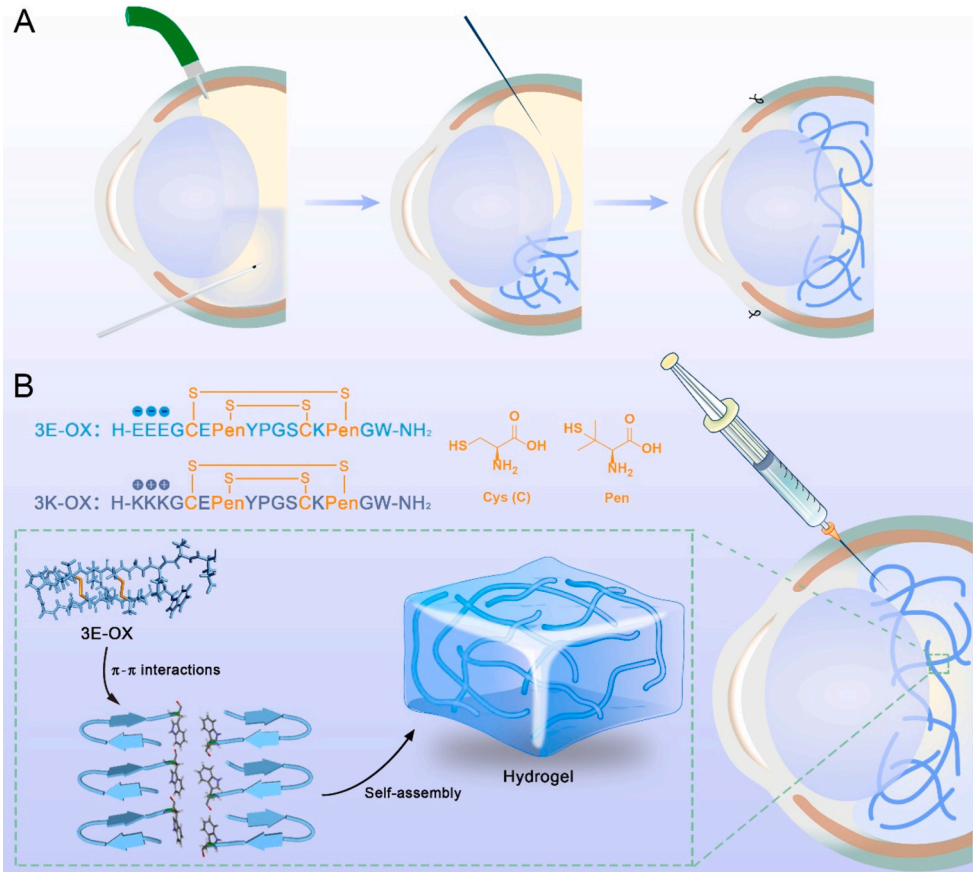

Fig. 1. Schematic overview of the preparation of 3E-OX hydrogel and its application for vitrectomized model in New Zealand rabbits. A) Schematic representations of vitrectomy procedure followed with hydrogel filling. B) Peptides self-assemble into hydrogel mainly through aromatic-aromatic interactions, serving as a vitreous substitute. The designed peptide sequences are also depicted.

applicable only in short-term use for intraocular toxicity [10,11]; Silicone oil (SO), the sole long-term vitreous endotamponade on the market, can lead to various sight-threatening conditions as cataracts, glaucoma, and retinal complications, necessitating close monitoring and subsequent removal surgery, thereby further increasing the socio-economic burdens [12]. Thus, an urgent need for the development of ideal biomaterials as vitreous substitutes is warranted.

An optimal vitreous substitute should have proximate properties of the natural human vitreous. Thus hydrogels, particularly peptide hydrogels driven by non-covalent interactions, are emerging as promising candidates due to their similarities with vitreous, such as high-water content, remarkable optical clarity, and exhibit properties that are biocompatible, injectable, and possess optimal viscoelasticity [13–16]. These materials have found versatile biomedical applications, spanning tissue engineering [17–21], drug delivery [22,23], cancer inhibition [24–27], personalized healthcare monitoring [28,29], and immunomodulation [30–32], with notable relevance in the management of ocular diseases. For example, Gao et al. developed an injectable antibody-loaded supramolecular hydrogel capable of prolonging the release time of anti-VEGF drugs, effectively inhibiting vascular proliferation in the retina and attenuating choroidal neovascularization [33]; Li and Huang et al. demonstrated the therapeutic efficacy of various peptide hydrogels in controlling ocular inflammation and their effectiveness in treating non-infectious uveitis [34–37]. Furthermore, Nishida and his colleagues reported a self-assembling peptide hydrogel capable of filling the vitreous cavity and remaining compatible for 3 months [38].

Inspired by these advancements, this research aims to explore the potential of peptide hydrogel with different charges as an ideal vitreous substitute. Previous research has highlighted the profound impact of surface charge on the biocompatibility and immunogenicity of biomaterials [39,40]. Consequently, optimizing surface charge is imperative to enhance biocompatibility and diminish immunogenicity for biomedical applications. In this work, we designed two peptide hydrogels, 3K-OX and 3E-OX, featuring positive and negative charges, respectively (Fig. 1). We systematically investigated their biocompatibility, rheological properties, and morphologies. Our in vitro studies revealed that hydrogel 3E-OX closely resembles the structure and functions of the native vitreous body, suggesting its suitability as a vitreous substitute. Subsequent animal studies, including assessments of intraocular pressure (IOP), slit lamp, B-ultrasound, optical coherence tomography (OCT), and histopathological examination, further confirmed the safety and biocompatibility of hydrogel 3E-OX, with minimal adverse effects observed. The work not only presents a compelling vitreous alternative but also provides valuable insights into the design of human vitreous substitutes.

2. Materials and methods

2.1. Materials

Rink Amide (AM) Resin, Fmoc-protected amino acids, and coupling reagents were purchased from CSBio (Shanghai) Ltd. Ethyldiisopropylamine (DIPEA) and trifluoroacetic acid (TFA) were supplied by Energy Chemical (Shanghai, China). L-glutathione oxidized (GSSG) was purchased from Sigma Aldrich (Shanghai, China). Calcein-AM/PI was purchased from Beyotime (Shanghai, China). All the solvents and reagents were used directly as received from commercial sources without further purification.

2.2. Animals

Twenty-four healthy adult New Zealand White rabbits (male, average weight of approximately 2.0–3.0 kg; Taiping Biological Technology Co. Ltd., Hunan, China, Certificate No. 1107302011000647) were used in this study. The living environment, diet, transportation, and experimental procedures of animals have followed the guidelines of the Association for Research in Vision and Ophthalmology, and are conducted by the approved protocols of the Institutional Animal Care and Use Committee at the 2nd Xiangya Hospital of Central South University (Approved No. 20231298).

2.3. Peptide synthesis

All the peptides were synthesized via standard Fmoc solid-phase peptide synthesis strategy using a CSBio synthesizer, with AM Resin and coupling by DIEA and HCTU. The resin-bound peptide was cleaved and side-chain deprotected using a cocktail of TFA/phenol/water/triisopropylsilane (88:5:5:2) for 3 h under a nitrogen atmosphere. The resin mixture was filtered and washed with excess ether. The crude peptide was obtained by concentrating the filtrate and precipitating it with cold ether. The crude product was purified by reverse-phase high-performance liquid chromatography (RP-HPLC). HPLC solvents comprised solvent A (0.1 % TFA in water) and solvent B (0.1 % TFA in 9:1 acetonitrile/water). The method employed was a linear gradient from 10 to 80 % solvent B over 30 min, then lyophilized to obtain dry powder. All purified reduced peptides were analyzed using analytical HPLC and MALDI-TOF MS.

2.4. Peptide oxidation

Reduced peptides (~1.0 mM) were dissolved in 100 mM phosphate buffer (pH 7.4) containing 2 equivalents GSSG. After incubation at 37 °C for 2 h, the final product of the oxidation reaction was monitored by analytical HPLC. The sample was purified by RP-HPLC and lyophilized to obtain dry powder.

2.5. Hydrogel preparation

In a typical experiment, 2.0 mg 3E-OX peptide was dissolved in 100 μL D.I. water, then adding 100 μL 0.2 ×PBS buffer (137 mM NaCl, 2.7 mM KCl, 10 mM Na_2HPO_4, 1.8 mM KH_2PO_4, pH 7.4) into peptide solution to trigger hydrogelation. Another 2.0 mg 3K-OX peptide was dissolved in 100 μL D.I. water and adding 100 μL BTP buffer (100 mM BTP, 300 mM NaCl, pH 7.4), then adjust the pH of the solution to 12–13 to trigger hydrogelation. The hydrogelation was evaluated by the inverted tube test as reported previously.

2.6. Circular dichroism (CD) spectroscopy

CD spectra were recorded (260–200 nm) using a Jasco-1500 spectrometer (Japan) under a nitrogen atmosphere. The peptide was prepared in the PBS buffer (pH 7.4, 13.7 mM NaCl, 0.27 mM KCl, 1 mM Na_2HPO_4, 0.18 mM KH_2PO_4) and BTP buffer (50 mM BTP, 150 mM NaCl, pH 7.4) at the concentration of 150 μM as previous described. The sample was placed evenly on the 1.0 mm thick quartz cuvette and scanned with a 1 nm interval three times. The resultant CD spectra were acquired after subtracting the solvent background.

2.7. Oscillatory rheology

The rheological properties, including the storage modulus (G') and the loss modulus (G"), were measured by a rheometer (MCR-92, Anton Paar, Austria) using a 15 mm parallel plate geometry. The 15 mm parallel plate geometry was lowered onto the hydrogel sample to a working gap of 0.5 mm, which was determined to provide good contact between the geometry and the hydrogel without damaging the sample (zero normal force). The testing stage was set to 37 °C and the standard silicon oil was used to prevent sample dehydration. The amplitude sweep test was carried out at an angular frequency of 6 rad s^{-1} and an amplitude range of 0.1 % ~ 100 % strain. The frequency sweep test was performed at a strain amplitude of 0.2 % strain (found to be within the linear viscoelastic region). The frequency ranges from 0.01 to 100 rad s^{-1} to measure the storage modulus (G') and loss modulus (G") of the hydrogel was measured. The shear thinning measurement is based on the time mode, and a 1000 % stress lasting for 1 min is given at the 60th minute to continue to detect the two modulus changes of the hydrogel for 60 min.

2.8. Transmission Electron microscopy

TEM images were acquired using a JEOL JEM-2100 PLUS microscope operating at an accelerating voltage of 80 kV. A 1.0 wt% uranyl acetate solution was employed as the staining agent. Briefly, 10 μL of diluted hydrogel was applied onto a carbon-coated copper mesh (200 mesh) for 1 min. The excess hydrogel was removed using filter paper, followed by rinsing with water and staining with uranyl acetate, each step repeated three times. Excess water and staining agents were removed with filter paper after each rinse, and the sample was air-dried at room temperature.

2.9. Cell viability assay

Adult retinal pigment epithelial cell line 19 (ARPE19), and human dermal fibroblast (NHDF) cells (5000 cells per well) were seeded in 96-well plates with 100 μL of DMEM medium, and Moorfields/Institute of Ophthalmology-Müller 1 (MIO-M1) cells (5000 cells per well) were seeded with 100 μL of DMEM-F12 medium supplemented with 10 % fetal bovine serum, 100 U mL^{-1} penicillin, and 100 μg mL^{-1} streptomycin. Following a 24-h incubation at 37 °C, 5 % CO_2, the culture medium was replaced with fresh serum-free medium containing 0.01-500 μM peptides diluted from 10 mM stock solution. The blank medium was used as a positive or negative control. After a 24-h incubation period, cells were washed and 100 μL of fresh serum-containing media was added to each well. 10 μL of (3-(4,5-Dimethylthiazol-2-yl)-2,5-diphenyl-tetrazolium bromide (MTT, 5 mg mL^{-1} in PBS) was added to each well, and samples incubated for 4 h, then added 10 % sodium dodecyl sulfate at 37 °C overnight to facilitate formazan crystal solubilization. Absorbance was recorded at 570 nm using a UV plate reader (Spectra Max M2). The absorbance of the negative controls was subtracted from each sample as a blank, and the percent viability was calculated as follows: (Absorbance peptide-treated cells / Absorbance untreated cells) × 100 %.

2.10. Scanning Electron microscope

SEM images were collected via a TESCAN MIRA3 LMH (Czech) at 0.5–30 KV accelerating voltage. The hydrogel sample was quickly frozen in a liquid nitrogen environment to crystallize the water inside the hydrogel and then lyophilized for at least 24 h to sublimate the ice crystals. The freeze-dried samples were then placed on a plate filled with liquid nitrogen, cut with a very fine blade to expose the cross-section, and finally sprayed with gold.

2.11. Transmittance measurement

Light transmittance of the hydrogel was assessed using a UV/vis spectrophotometer (UV-1900i, Shimadzu, Japan) across a wavelength spectrum ranging from 400 to 800 nm, with 0.2 × PBS serving as the blank sample.

2.12. Refractive index measurement

The refractive indexes of 3E-OX hydrogels and isolated pig-eye vitreous bodies were determined using an Abbe refractometer (WYA—2S, INESA, Shanghai, China), with water serving as the blank sample.

2.13. Cytocompatibility measurement

Three-dimensional (3D) cell culture images were captured using a CLSM980 microscope (Zeiss, Germany). Initially, the peptide was sterilized with UV light for 30 min. To encapsulate the cells, the oxidized peptide was dissolved in 285 mM sucrose and combined with cell suspensions (50,000 cells) prepared in a serum medium. The mixture was then transferred to 96-well plates and allowed to incubate for 3 h. Subsequently, 100 μL of complete medium was added, and the Live/Dead assay was employed to evaluate cell viability within the gels after 24 h. Finally, fluorescence imaging was conducted on the CLSM for *Z*-axis scanning.

2.14. Permeability assessment

A 200 μL aliquot of hydrogel 3E-OX was evenly spread on the bottom of a glass bottle, allowed to stabilize for 3 h, and then supplemented with 1 mL of NBD dye diluted in PBS. Photographs were captured at 1, 5, and 60-min intervals, respectively. To assess hydrogel permeability, the NBD dye was left in contact with the hydrogel for 24 h, after which it was removed and replaced with 1 mL of fresh PBS solution. Subsequently, photographs were taken at 1, 5, 10, 15, 30, and 60-min intervals. The PBS solution was replaced with a fresh solution after each imaging session.

2.15. Fluorescence assays

The fluorescence spectrum was recorded using an F2500 fluorescence spectrophotometer (Hitachi, Tokyo, Japan) with an excitation wavelength set to 280 nm. The samples were evenly placed in a 10 mm-thick quartz cuvette, and the emission spectra were recorded between 300 nm and 450 nm. Finally, the solvent background was subtracted to obtain the corrected fluorescence spectrum.

2.16. UV/Vis spectroscopy

Different concentrations of peptide solution of 3E-OX were prepared in 0.1 × PBS buffer and incubated at 37 °C for 24 h. The UV/vis spectra (250–600 nm) were then recorded using a UV 1900i UV-VIS spectrophotometer (Shimadzu, Japan).

2.17. Vitrectomy surgery

After the exclusion of ocular lesions, compound tropicamide eye drops were used to dilate the rabbits' pupils 30 min before surgery. General anesthesia was performed with a combination of intramuscular Chlorpromazine (30 mg kg^{-1}) and 3 % intravenous Pentobarbital sodium (1 mg kg^{-1}). A 2-port, 23-gauge pars-plana vitrectomy surgery was performed by the same experienced surgeon. Following the removal of as much vitreous as feasible, 1.0–1.5 mL of Lactate Ringer's solution, silicone oil, 3E-OX hydrogel, and 3K-OX hydrogel were injected into each of the rabbit eyes. Postoperative anti-inflammatory and anti-infective treatments were administered for 14 days.

2.18. IOP measurements

IOP was measured by the TonoVet tonometer (Icare, Finland) on the center of the cornea. For each rabbit, preoperative and postoperative (1, 3, 7, 15, and 30 days after surgery) IOP data were collected.

2.19. Slit lamp examination

Compound tropicamide eye drops were used to dilate the pupils 20 min before examination. The anterior and posterior segments were non-invasively recorded by a slit-lamp (Model BL-66B, Bolan Optical Electric Co. Ltd., Shanghai, China) and a 90D non-contact lens (Volk Optical Inc.). For each rabbit, preoperative and postoperative (1, 3, 7, 15, and 30 days after surgery) data were collected.

2.20. Optical coherence tomography examination

The real-time spectral-domain optical coherence tomography (Heidelberg Engineering) was used to record the structure of the retina and choroid preoperatively and postoperatively at days 7, 15, and 30 after surgery. Using the Fiji ImageJ software for retinal and choroid layer thickness analysis.

2.21. Optical coherence tomography angiography (OCTA) examination

The Swept Source Optical Coherence Tomography System (TOWARDS Π, Beijing, China) was used to quantify the retinal vascular perfusion area at day 15 after surgery. Using the Fiji ImageJ software for retinal vascular perfusion area, VAD, and VDI analysis. For the vessel area density (VAD) and vessel diameter index (VDI) analysis, the images were binarized and skeletonized. VAD = black pixels of selected area in the binary image / the total pixels in the binary image. VDI = black pixels of a selected area in the binary image / black pixels of a selected area in the skeleton image.

2.22. B-mode ultrasonography examination

Using a B-mode ultrasonography device (AVISO) to observe the turbidity degree of the vitreous cavity. For each rabbit, preoperative and postoperative (3, 7, 15, and 30 days after surgery) data were collected. The Fiji ImageJ software was used for the gray value analysis.

2.23. Electroretinogram (ERG) examination

All the rabbits were dark-adapted and dilated 30 min before examination. After general intravenous anesthesia, ERG examinations were recorded by the MonPackONE electrophysiological equipment (METRO VISION). The ground electrode was fixed subcutaneously on the forehead of the rabbit, the reference electrode was fixed under the skin of both ears, and the corneal electrode was placed on the corneal surface. The full-field ERG was measured, including dark-adapted (DA) 0.01 ERG, DA 3.0 ERG, DA oscillatory potentials, light-adapted (LA) 3.0 ERG and LA 30 Hz flicker ERG. Each examination was repeated at least three times.

2.24. Gross anatomy examination

All of the rabbits were subjected to euthanasia and their eyeballs were enucleated. The anterior section of the eyeballs was meticulously dissected, and the thorough gross appearance of the lens and vitreous cavity contents were observed. The posterior portion was incised, allowing for the examination of the gross morphology of the retina.

2.25. Histopathological examination

All the rabbits were euthanized. The eyeballs were enucleated and immersed in FAS specimen fixative (Servicebio, Wuhan) for 24 h. Then the samples were cut longitudinally and embedded in paraffin. The paraffin block was cut at 5 μm with a microtome (Leica RM2016) and further stained with Hematoxylin-Eosin (H&E) stain.

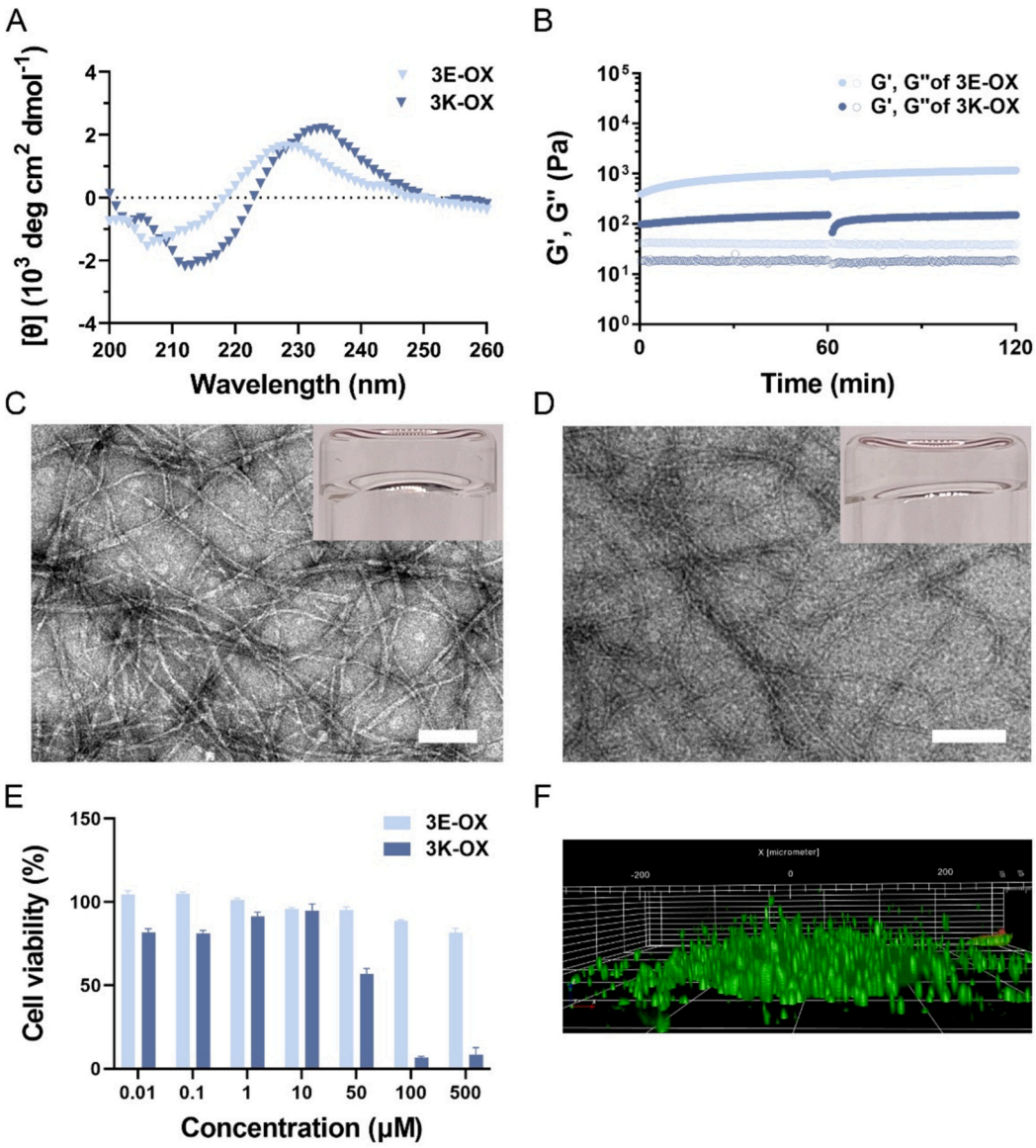

Fig. 2. Characterization of peptide assemblies and their hydrogels. A) CD spectra of 150 μM 3E-OX in PBS buffer (27.4 mM NaCl, 0.54 mM KCl, 2 mM Na_2HPO_4, 0.36 mM KH_2PO_4, pH 7.4) and 3K-OX in BTP buffer (50 mM BTP, 150 mM NaCl, pH 7.4). B) Rheological measurements tracking the storage moduli (G') and loss moduli (G") of hydrogel 3E-OX and 3K-OX over time, show the shear-thin recovery property. TEM images of 1.0 wt% 3E-OX C) and 3K-OX D) hydrogels, scale bar = 100 nm. E) Cytotoxicity of 3E-OX and 3K-OX against ARPE19 cells after 24 h of incubation. F) Live/Dead assay of ARPE19 cells after seeding into 1.0 wt% 3E-OX hydrogel for 24 h.

2.26. Statistical methods

Data analysis was performed by SPSS version 28.0. The quantitative data were presented as mean ± standard deviation (SD). Multiple *t*-tests were used to analyze the data for intraocular pressure, B-mode ultrasound grayscale value, retinal thickness, and choroidal thickness. VAD and VDI were statistically analyzed by paired t-test. Due to heteroscedasticity in ERG wave amplitude data, variance analysis with the Dunnett T3 test was used for statistical analysis. Differences were considered statistically significant at $P < 0.05$.

3. Results and discussion

3.1. Molecular design

In our previous study, we reported a thiol-rich peptide GCE(*Pen*)YPGSCK(Pen)GW (R1), where "Pen" denotes a Cys-like amino acid with β, β-dimethyl substitution (shown in Fig. 1B). This peptide folded into an amphiphilic β-hairpin conformation upon oxidation and formed two hetero-disulfide bonds, leading to the formation of a transparent hydrogel with high compatibility [41]. Molecular simulations demonstrated the essential role of the tryptophan residue in facilitating hydrogel formation. To explore the influence of surface charges on the suitability of peptide hydrogel as a vitreous substitute, we design two peptides, 3E and 3K, by incorporating three glutamic acid residues (E, negative charge) and three lysine residues (K, positive charge) at the N terminal of sequence (Fig. 1B). Among the 20 natural amino acids, both E and D possess negative charges, while K, R and H possess positive charges. Here, we chose E and K to regulate the charge of peptides. Peptides 3E-OX and 3K-OX were obtained by oxidizing peptides 3E and 3K, respectively, following our previously reported method (**Fig. S1 and Fig. S2**) [41]. Compared to linear peptide-based hydrogels, the disulfide-rich peptide hydrogels in this work offer greater stability under physiological conditions due to their cyclic structures. This increased stability can be advantageous for in vivo applications [42,43].

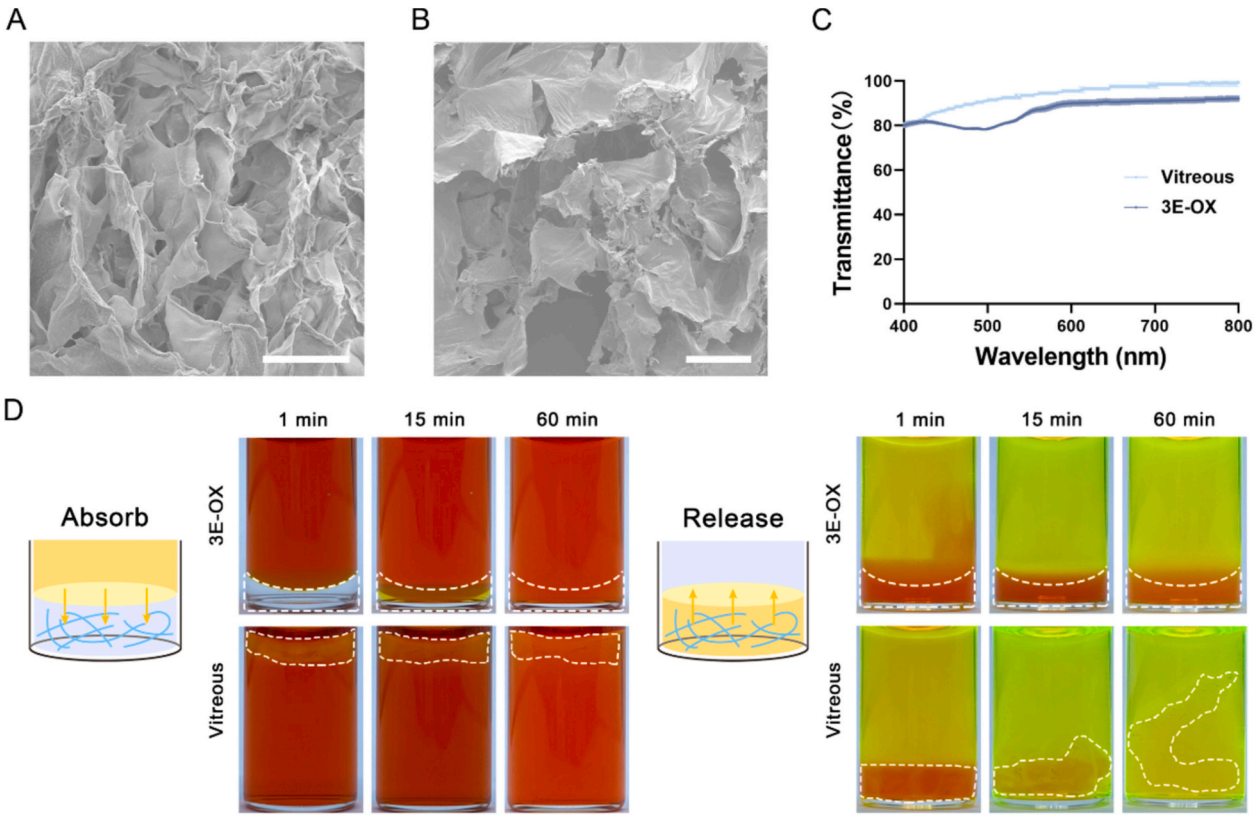

Fig. 3. Physical properties of the peptide hydrogel. SEM images of A) 1.0 wt% hydrogel 3E-OX and B) vitreous, scale bars are 20 μm and 10 μm from left to right. C) transmittance comparison between the native vitreous and hydrogel 3E-OX. D) Permeability assessment of fluorescein sodium dye penetrating in (left) and out (right) of hydrogel 3E-OX and native vitreous at various time points.

3.2. Characterization of peptide hydrogels

To examine their self-assembly behaviors, CD was used to elucidate the conformational changes of these peptides under physiological conditions. As shown in Fig. 2A, both 150 μM solutions of 3E-OX and 3K-OX exhibited a β-sheet-like structure, indicating the formation of disulfide bonds promotes the adoption of a β-hairpin conformation by the peptide, thereby facilitating peptide self-assembly and hydrogelation. In contrast, the linear peptides display a random coil structure under the same conditions. Subsequently, fluorescence spectroscopy was utilized to further characterize their self-assembly behavior. **Fig. S3** illustrates a blue shift in the maximum emission wavelength from 351 nm to 348 nm when 3K-OX was prepared in a bis-tris propane (BTP) buffer. Additionally, a decrease in the fluorescence intensity of 3K-OX in BTP buffer compared to that in water was also observed, suggesting reduced solvent exposure of tryptophan residues and indicating the occurrence of self-assembly events in the BTP buffer. Similar observations were made for 3E-OX [44]. Furthermore, we employed UV/vis spectroscopy to evaluate the mechanism of self-assembly. A new peak appeared around 355 nm when the concentration of 3E-OX increased to 300 μM, indicating the π-π interactions from the indole ring in tryptophan residues (**Fig. S4**). Collectively, these results suggest that tryptophan residue is essential for the self-assembly of these peptides. Then, peptide solutions (2.0 %, w v^{-1}) were prepared in glass vials by dissolving 2 mg of 3E-OX or 3K-OX in 100 μL deionized water. To this solution, an equal volume of 0.2×phosphate buffered solution (PBS) or BTP buffer (100 mM BTP, 300 mM NaCl, pH 7.4) was added to initiate the hydrogelation. It is noteworthy that the hydrogel intended for vitrectomy should undergo a buffer exchange process with PBS.

The rheological properties of the hydrogel were evaluated using oscillatory rheology. As shown in Fig. 2B, both 3E-OX and 3K-OX underwent self-assembly into hydrogels within the initial 60 min, with G′ values of approximately 1.0×10^3 and 1.5×10^2 Pa, respectively. The different rigidity of these two hydrogels may be caused by different net charges of these peptides under physiological conditions. Subsequently, a large strain (1000 %) was applied for 1 min to thin the hydrogel 3E-OX, which recovered completely within a few minutes when the applied strain was reduced to 0.2 %, indicative of its shear-thin recovery properties. A similar trend was observed in gel 3K-OX. This behavior indicates that the hydrogel could be administered as a liquid and rapidly gel upon reaching the vitreous cavity. Additionally, Fig. 2C and Fig. 2D illustrate that both peptides form transparent hydrogels, and transmission electron microscopy (TEM) images reveal a network rich in nanofibers constituting the morphology of the hydrogel matrix. The measured width of the fibers in hydrogels 3E-OX and 3K-OX are around 4.9 nm and 4.8 nm, respectively. It should be noted that there are some wider fibers in the TEM image of hydrogel 3E-OX, which may be attributed to the superposition of two or more single fibers (**Fig. S5**).

The cytocompatibility of hydrogel is paramount for its potential application as a vitreous substitute. Hence, we evaluated the cytotoxicity of these peptides against ARPE19, NHDF, and MIO-M1 cell lines. The results in Fig. 2E and **Fig. S6** show that peptide 3E-OX demonstrates minimal cytotoxicity towards both ARPE19, NHDF, and MIO-M1 cells, whereas peptide 3K-OX exhibits significant cytotoxicity towards both cell lines when the concentration exceeds 100 μM. The poor biocompatibility observed in 3K-OX may be attributed to the excess positively charged lysine residues, which could potentially disturb the negatively charged cell membrane, leading to cytotoxicity. Consequently, peptide 3K-OX is unsuitable for further investigation as a vitreous substitute. To further validate the biocompatibility of hydrogel 3E-OX, we utilized this hydrogel as a 3D scaffold for cell culture. As illustrated in Fig. 2F, ARPE19 cells maintained high viability within the hydrogel, indicating this peptide-based biomaterial has minimal negative impact on cell viability.

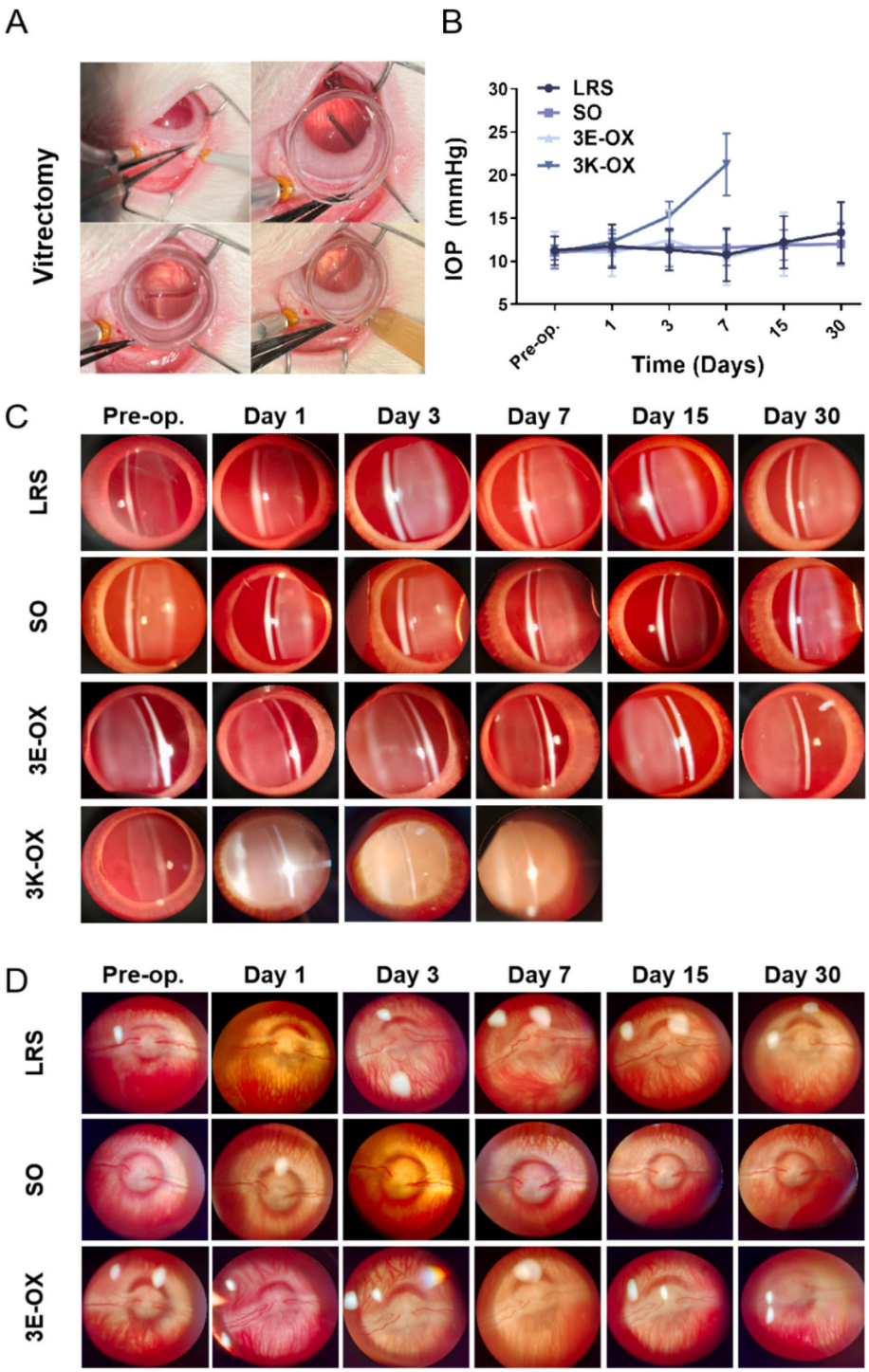

Fig. 4. Safety assessment of peptide hydrogels through intraocular pressure measurement and anatomical examination. A) Schematic depiction of standard pars plana vitrectomy procedures and hydrogel injection. B) Monitoring of post-injectional intraocular pressure over time. Slit-lamp photographs illustrating the anterior segment C) and fundoscopy images D) at various time points following injection. IOP is presented as mean ± SD. Multiple *t*-tests were conducted to analyze intraocular pressure data. Rabbit groups consisted of $n = 3$–6 individuals.

3.3. *Physical properties of hydrogel 3E-OX*

The native vitreous, comprising 98 % water along with a network of collagen and proteoglycans, shares a striking resemblance to hydrogel structures [45]. Given its potential as an ideal vitreous substitute, peptide hydrogel 3E-OX is anticipated to resemble the morphologies of the vitreous body. To verify this hypothesis, scanning electron microscopy (SEM) was utilized to visualize the morphologies of the hydrogel 3E-OX matrix alongside the vitreous body of the eye. As shown in Fig. 3A and Fig. 3B, both hydrogel 3E-OX and vitreous body exhibit highly similar porous structures. Optical transparency is another crucial criterion for a vitreous substitute. Fig. 3C demonstrates that hydrogel 3E-OX exhibits acceptable transmittance across the visible light wavelength range (400–800 nm), which is very close to the native vitreous body. Additionally, the refractive index of hydrogel 3E-OX closely mirrors that of the native vitreous body, ranging from 1.3395 to 1.3410 at 552 nm,

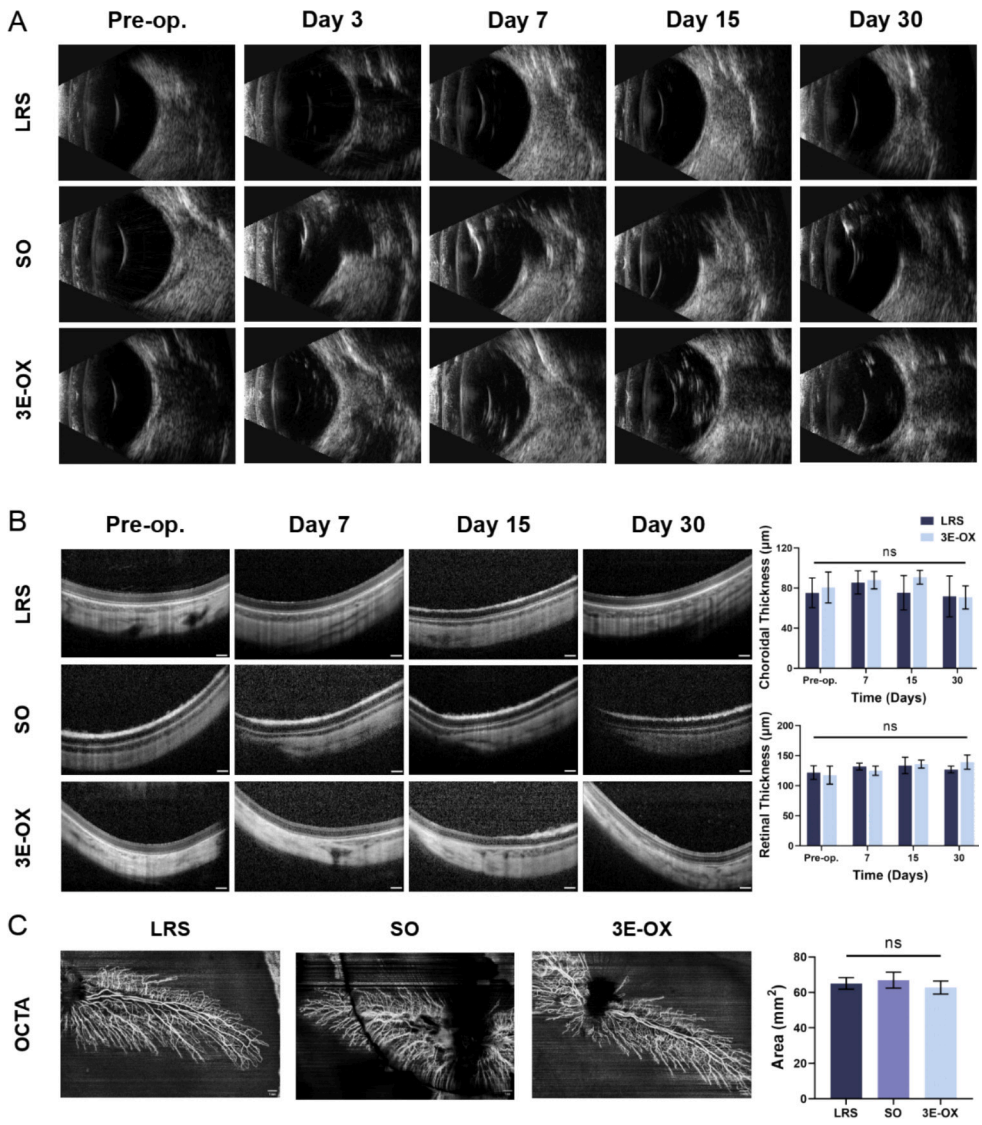

Fig. 5. Structural safety assessment of 3E-OX using B-ultrasound, OCT, and OCTA imaging. A) Representative B-ultrasound images over time indicate a flat fundus in all rabbit eyes across the LRS, SO, and 3E-OX groups. B) Representative images of OCT at various time points reveal comparable structural integrity of the retina and choroid between the 3E-OX and control groups, scale bar = 200 μm. Quantification of retinal and choroidal thickness over time shows no statistically significant changes within 30 days. Retinal and choroidal thickness are presented as mean ± SD. Multiple t-tests were used to analyze the data for retinal thickness and choroidal thickness, with n = 3–6 in rabbit groups. C) Representative OCTA images at day 15 illustrate normal blood vessel distribution across all groups, scale bar = 1 mm. The quantification analysis of the retinal vascular perfusion area suggests no statistical differences among the three groups, with n = 3 in rabbit groups.

thereby mitigating potential postoperative refractive shifts (**Fig. S7**) [6]. Moreover, physical properties such as pH and density were evaluated to assess the compatibility of peptide hydrogel as a vitreous substitute. As summarized in **Table S1**, the pH of hydrogel 3E-OX remains within physiological conditions (7.0–7.25), similar to the pH of the human vitreous (7.0–7.4) [6]. Similarly, the density of hydrogel 3E-OX (1.0669–1.1383 g cm^{-3}) closely approximates that of the human vitreous (1.0053–1.0089 g cm^{-3}) [6]. The slightly denser than water makes 3E-OX a suitable endotamponade that eliminates the need for patients to remain prone for long periods after surgery. Meanwhile, an ideal vitreous substitute should exhibit excellent permeability to facilitate metabolic exchange and maintain normal intraocular microenvironment and homeostasis [46]. Fluorescein sodium, a model molecule with a molecular weight of 356 Da, was utilized to assess the permeability of hydrogel 3E-OX. As illustrated in Fig. 3D, fluorescein sodium rapidly diffused into the hydrogel, permeating the entire hydrogel matrix within 60 min, similar to the permeability observed in the native vitreous body. Furthermore, the release rate of trapped small molecules within the hydrogel was examined. Fig. 3D's right panel indicates a gradual release of fluorescein sodium release into the surrounding environment over 60 min, slightly slower than that of the native vitreous body. Permeability tests with silicone oil (**Fig. S8**) demonstrated poor permeability, while a high molecular weight red fluorescent protein (mCherry, M.W.: 28 kDa) exhibited limited diffusion into hydrogel 3E-OX within a short time, similar to the native vitreous body (**Fig. S9**). This limited permeability of large molecules may contribute to maintaining intraocular microenvironment stability [47]. These findings collectively suggest that hydrogel 3E-OX possesses excellent permeability of small molecule transportation while impeding macromolecule penetration, indicating its potential as a promising vitreous substitute. In addition, we also evaluated the stability of hydrogel 3E-OX in vitro. As shown in **Fig. S10**, 3E-OX maintained high stability during the experimental period (at least one week) after being covered with 1 mL PBS buffer and shaken at 37 °C. Notably, **Fig. S11** showed that peptide 3E-OX can still be observed three months after implantation, further suggesting its high stability in vivo.

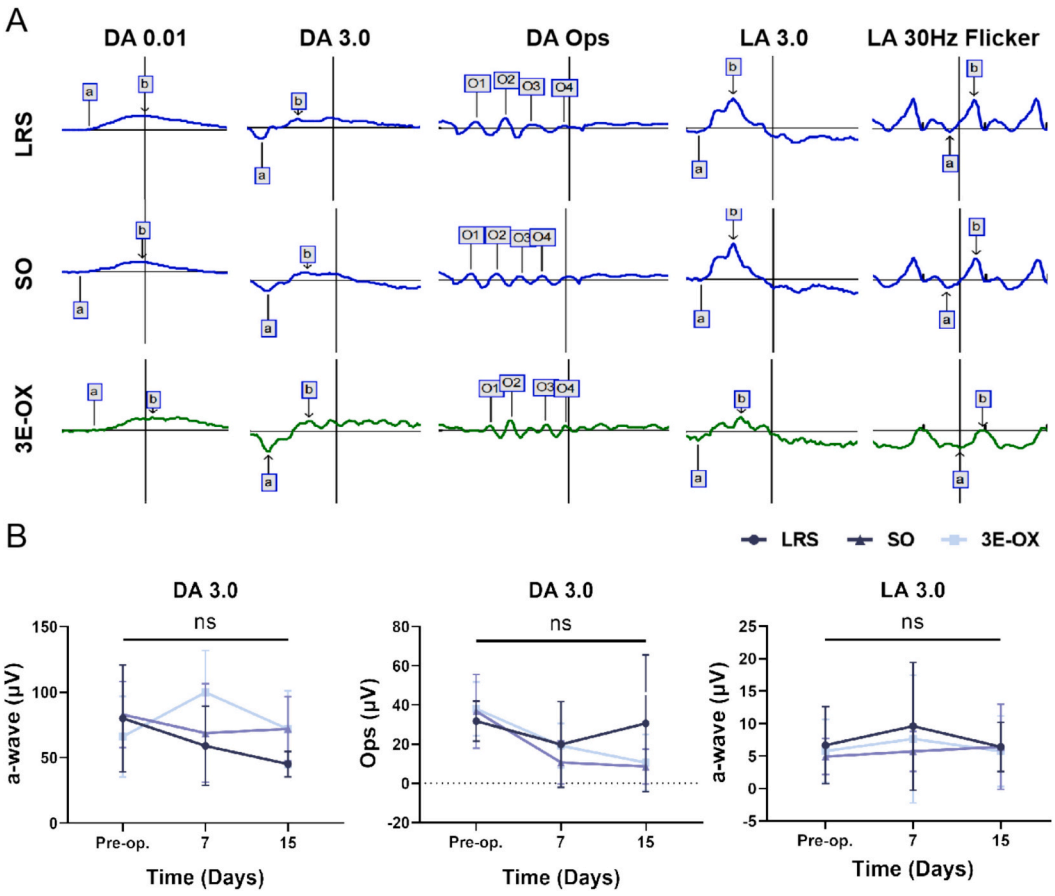

Fig. 6. Functional assessment of rabbits at 15 days post-implantation. A) Representative images of ERG on day 15. B) Quantitative analysis of the ERG amplitude showed no significant difference between the 3E-OX group and control groups on day 15. ERG wave amplitude data were analyzed using variance analysis with the Dunnett T3 test. Rabbit groups consisted of $n = 3$–6.

3.4. Evaluation of biocompatibility of peptide hydrogels in vivo

To assess the in vivo biocompatibility of hydrogel 3E-OX, we established a vitrectomized endotamponade model in New Zealand white rabbits. The gel was injected into the vitreous cavity (Fig. 4A and **Fig. S12**), with LRS and SO serving as control substances, as they are commonly used as vitreous substitutes in clinical practice. All of these vitreous endotamponades were injected into the vitreous cavity only once on the day of surgery. Subsequently, we monitored the structure and function of the rabbit eyes for one month to evaluate biocompatibility. Firstly, our findings revealed that the peptide hydrogel can be administrated more easily through a 23G incision compared to SO, with less resistance during injection, and the procedures being simpler and more accessible. As shown in Fig. 4B, IOP fluctuations remained within the normal range (11-21 mmHg) for all groups except the 3K-OX group (>21 mmHg). Notably, intraocular toxicity was observed in the 3K-OX group on the first week post-surgery, characterized by the lens and vitreous opacity (Fig. 4C and **Fig. S13**), fundus invisibility (**Fig. S14**), and dissolved retina (**Fig. S15**). This suggests that positively charged hydrogel may trigger a reaction with intraocular tissue, leading to severe intraocular inflammation. In contrast, rabbits implanted with LRS, SO, and 3E-OX hydrogel exhibited no significant inflammatory reactions in either the anterior or posterior segments. Furthermore, all tamponades remained clean and optically clear within the vitreous cavity (Fig. 4C and Fig. 4D), indicating superior biocompatibility in these three groups warranting further investigation.

To further evaluate the influence of hydrogel on intraocular tissues and retina, we employed B-ultrasound, OCT, OCTA, and H&E staining to assess the structural changes in the operated eyes. The B-ultrasound results (Fig. 5A) revealed a consistently flat fundus treated with intraocular LRS, SO, and 3E-OX, indicating proper adhesion of the retina to the posterior eye wall. Notably, in the 3E-OX group, a transient increase in the gray value of the vitreous cavity was observed, returning to baseline levels by day 30. This suggests potential ultrasound scatter at the gel-liquid interface and/or gradual degradation of the hydrogel over time. Similar transient alternations were noted in the LRS group, statistically comparable to 3E-OX (**Fig. S16**). Recognizing such transient changes is critical as they may affect ultrasound interpretations, offering valuable insights into hydrogel behavior and biocompatibility within the ocular environment. Furthermore, 3E-OX hydrogel exhibited an advantage over SO in preventing the false enlargement of the vitreous cavity in ultrasonography, enhancing the accuracy of retinal assessment, and minimizing misleading artifacts. However, in the 3K-OX group, the retinal detachment was found on day 7 after surgery (**Fig. S13**), suggesting a compromised ocular environment associated with this positively charged hydrogel.

The OCT imaging in Fig. 5B revealed consistent and clear retina and choroidal structures in both 3E-OX and control groups at each time point. Measurements of retinal and choroidal thickness remained unchanged up to day 30, suggesting the safety of 3E-OX on these structures. More importantly, OCTA allowed noninvasive quantification of retinal vascular perfusion area, VAD, and VDI (**Fig. S17** and **Fig. S18**), marking the first study to evaluate the effects of vitreous substitutes on retinal vasculature. As depicted in Fig. 5C, within 15 days post-surgery, the distribution of blood vessels appeared normal in all three groups, indicating that 3E-OX did not cause short-term abnormalities in the retinal vascular system. Gross evaluation on day 30 revealed no other anatomical defects in the 3E-OX group (**Fig. S15**), and the

histopathological examination confirmed intact and articulated retinal layers in the hydrogel-injected eyes (**Fig. S19**). Collectively, hydrogel 3E-OX exhibited superior performance than 3K-OX, without significant inflammatory and toxic response, thus warranting further investigation as a vitreous substitute. Since hyaluronic, a component of the vitreous body bears a substantial negative charge, the excess positively charged lysine residues may interact with it and contribute to its toxicity.

Full-field electroretinography served as a valuable, objective tool for assessing the overall electrical activity of the retina, offering insights into the functionality of retinal visual formation and microcirculation [48]. As depicted in the ERG results presented in Fig. 6, no notable differences were observed between the eyes injected with the hydrogel and the control eyes on day 15. This suggests that the retinal cells exhibited good tolerance to the presence of the hydrogel over this period. These findings indicate that the 3E-OX hydrogel can provide a supportive function for at least 15 days, a critical duration for facilitating retinal self-repair processes. This implies that the hydrogel serves as a suitable substrate for maintaining retinal integrity and function during the crucial initial phases of healing and regeneration [49]. Such support may potentially enhance the overall efficacy of therapeutic interventions aimed at promoting retinal health and recovery.

4. Conclusion

The challenges presented by current vitreous substitutes significantly hamper the post-vitrectomy prognosis of vitreoretinal diseases. This study has developed a novel self-assembling peptide hydrogel (3E-OX), featuring a three-dimensional network structure and the ability to hold large amounts of water. This constructed peptide hydrogel closely mimics native vitreous characteristics, exhibiting excellent optical clarity, porous structures, and high permeability facilitating metabolic exchange, and biocompatibility. Compared to clinical alternatives and synthetic polymer hydrogels, the hydrogel 3E-OX offers several distinct advantages: i. Excellent biocompatibility stemming from its primary composition of amino acids [50,51]; ii. Shear-thinning recovery properties, allowing injection through small-gauge incisions in the eye, while maintaining optimal mechanic strength post-injection [52]; iii. Simplified hydrogel preparation, involving the straightforward mixing of peptide solution with a physiological buffer. iv. Complete and harmless degradation, which avoids the risk and challenge of removing unreacted monomers, dopant ions, and residual solvents [53]. Based on recent work on peptide self-assembly, it is worth further exploring the mechanism of hydrogel 3E-OX formation to provide a deeper understanding of engineering peptide hydrogels in the future [54–56].

In summary, we thoroughly investigated the potential for intraocular use of hydrogel 3E-OX by characterizing its physicochemical properties. Furthermore, comprehensive assessments of the short-term biocompatibility of 3E-OX were conducted at both cellular and animal levels. Notably, we pioneered the utilization of whole-field scanning optical coherence tomography to perform retinal microvascular detection in non-pigmented rabbits. This novel approach enabled us, for the first time, to quantitatively evaluate the microvascular effects of intraocular tamponade materials. This advancement represents a crucial verification method for assessing the safety and applicability of such materials. Overall, our findings not only introduce a novel method for evaluating the performance of vitreous substitutes but also provide a promising alternative for their application in clinical settings.

CRediT authorship contribution statement

Yuting Cai: Writing – original draft, Methodology, Formal analysis, Data curation. **Yatong Xiang:** Writing – original draft, Methodology, Investigation, Data curation. **Huilei Dong:** Writing – review & editing, Validation, Methodology. **Wenjing Huang:** Methodology, Data curation. **Chenguang Zhao:** Methodology. **Dan Yuan:** Writing – review & editing, Validation. **Yun Li:** Writing – review & editing, Supervision, Funding acquisition, Conceptualization. **Junfeng Shi:** Writing – review & editing, Supervision, Funding acquisition, Conceptualization.

Declaration of competing interest

All the authors have no conflicts to declare.

Acknowledgments

This work was supported by the National Natural Science Foundation of China (No. 82171087 to Y.L, No. 22307096 to H.D), the National Youth Talent Support Program (202309460011 to J.S), Natural Science Foundation of Hunan (2022JJ10008 to J.S, No. 2023JJ70021 to Y.L), Guangdong Basic and Applied Basic Research Foundation (2024A1515011057 to J.S), Science and Technology and Development Foundation of Shenzhen (JCYJ20230807122008016 to J.S).

Appendix A. Supplementary data

Supplementary data to this article can be found online at https://doi.org/10.1016/j.jconrel.2024.10.016.

Data availability

The date will be made available on request.

References

[1] C. Gilbert, A. Foster, Childhood blindness in the context of VISION 2020–the right to sight, Bull. World Health Organ. 79 (2001) 227–232.
[2] T. Chan-Ling, G.A. Gole, G.E. Quinn, S.J. Adamson, B.A. Darlow, Pathophysiology, screening and treatment of ROP: a multi-disciplinary perspective, Prog. Retin. Eye Res. 62 (2018) 77–119.
[3] K. Ogurtsova, J.D. da Rocha Fernandes, Y. Huang, U. Linnenkamp, L. Guariguata, N.H. Cho, D. Cavan, J.E. Shaw, L.E. Makaroff, IDF diabetes atlas: global estimates for the prevalence of diabetes for 2015 and 2040, Diabetes Res. Clin. Pract. 128 (2017) 40–50.
[4] W.L. Wong, X. Su, X. Li, C.M. Cheung, R. Klein, C.Y. Cheng, T.Y. Wong, Global prevalence of age-related macular degeneration and disease burden projection for 2020 and 2040: a systematic review and meta-analysis, Lancet Glob. Health 2 (2014) e106–e116.
[5] F. Confalonieri, N. Josifovska, G. Boix-Lemonche, I. Stene-Johansen, R. Bragadottir, X. Lumi, G. Petrovski, Vitreous substitutes from bench to the operating room in a translational approach: review and future endeavors in vitreoretinal surgery, Int. J. Mol. Sci. 24 (2023) 3342.
[6] I. Yadav, S.D. Purohit, H. Singh, S. Bhushan, M.K. Yadav, T. Velpandian, R. Chawla, S. Hazra, N.C. Mishra, Vitreous substitutes: An overview of the properties, importance, and development, journal of biomedical materials research, Part B, Applied Biomaterials 109 (2021) 1156–1176.
[7] T.T. Kleinberg, R.T. Tzekov, L. Stein, N. Ravi, S. Kaushal, Vitreous substitutes: a comprehensive review, Surv. Ophthalmol. 56 (2011) 300–323.
[8] K. Wang, Z. Han, Injectable hydrogels for ophthalmic applications, Journal of controlled release : official journal of the Controlled Release Society 268 (2017) 212–224.
[9] M.J. Colthurst, R.L. Williams, P.S. Hiscott, I. Grierson, Biomaterials used in the posterior segment of the eye, Biomaterials 21 (2000) 649–665.
[10] C. Mondelo-García, E. Bandín-Vilar, L. García-Quintanilla, A. Castro-Balado, E. M. Del Amo, M. Gil-Martínez, M.J. Blanco-Teijeiro, M. González-Barcia, I. Zarra-Ferro, A. Fernández-Ferreiro, F.J. Otero-Espinar, Current situation and challenges in vitreous substitutes, Macromol. Biosci. 21 (2021) e2100066.
[11] G.A. Peyman, J.A. Schulman, B. Sullivan, Perfluorocarbon liquids in ophthalmology, Surv. Ophthalmol. 39 (1995) 375–395.
[12] Y. Chen, V.R. Kearns, L. Zhou, T. Sandinha, W.C. Lam, D.H. Steel, Y.K. Chan, Silicone oil in vitreoretinal surgery: indications, complications, new developments and alternative long-term tamponade agents, Acta Ophthalmol. 99 (2021) 240–250.
[13] F. Baino, Towards an ideal biomaterial for vitreous replacement: historical overview and future trends, Acta Biomater. 7 (2011) 921–935.
[14] K. Naik, L.C. Du Toit, N. Ally, Y.E. Choonara, Advances in polysaccharide- and synthetic polymer-based vitreous substitutes, Pharmaceutics 15 (2023) 566.
[15] X. Du, J. Zhou, J. Shi, B. Xu, Supramolecular Hydrogelators and hydrogels: from soft matter to molecular biomaterials, Chem. Rev. 115 (2015) 13165–13307.
[16] R.C. Cooper, H. Yang, Hydrogel-based ocular drug delivery systems: emerging fabrication strategies, applications, and bench-to-bedside manufacturing considerations, Journal of controlled release : official journal of the Controlled Release Society 306 (2019) 29–39.

[17] C.M. Madl, S.C. Heilshorn, Bioorthogonal strategies for engineering extracellular matrices, Adv. Funct. Mater. 28 (2018) 1706046.
[18] G. Yazdanpanah, X. Shen, T. Nguyen, K.N. Anwar, O. Jeon, Y. Jiang, M. Pachenari, Y. Pan, T. Shokuhfar, M.I. Rosenblatt, E. Alsberg, A.R. Djalilian, A light-curable and tunable extracellular matrix hydrogel for in situ suture-free corneal repair, Adv. Funct. Mater. 32 (2022) 2113383.
[19] C. Zhao, S. Tian, Q. Liu, K. Xiu, I. Lei, Z. Wang, P.X. Ma, Biodegradable nanofibrous temperature-responsive gelling microspheres for heart regeneration, Adv. Funct. Mater. 30 (2020) 2000776.
[20] X. Wu, M. Yan, J. Shen, Y. Xiang, K. Jian, X. Pan, D. Yuan, J. Shi, Enhancing calvarial defects repair with PDGF-BB mimetic peptide hydrogels, Journal of controlled release : official journal of the Controlled Release Society 370 (2024) 277–286.
[21] X. Ren, J. Wei, X. Luo, Y. Liu, K. Li, Q. Zhang, X. Gao, S. Yan, X. Wu, X. Jiang, M. Liu, D. Cao, L. Wei, X. Zeng, J. Shi, HydrogelFinder: A Foundation Model for Efficient Self-Assembling Peptide Discovery Guided by Non-Peptidal Small Molecules, Advanced Science (Weinheim, Baden-Wurttemberg, Germany) vol. 11 (2024) e2400829.
[22] C. Zhu, T. Li, Z. Wang, Z. Li, J. Wei, H. Han, D. Yuan, M. Cai, J. Shi, MC1R peptide agonist self-assembles into a hydrogel that promotes skin pigmentation for treating vitiligo, ACS Nano 17 (2023) 8723–8733.
[23] J. Zhou, Y. Cai, T. Li, H. Zhou, H. Dong, X. Wu, Z. Li, W. Wang, D. Yuan, Y. Li, J. Shi, Aflibercept loaded eye-drop hydrogel mediated with cell-penetrating peptide for corneal neovascularization treatment, Small (Weinheim an der Bergstrasse, Germany) 20 (2024) e2302765.
[24] J. Shi, X. Du, D. Yuan, J. Zhou, N. Zhou, Y. Huang, B. Xu, D-amino acids modulate the cellular response of enzymatic-instructed supramolecular nanofibers of small peptides, Biomacromolecules 15 (2014) 3559–3568.
[25] Q. Wang, X. Yang, R. Yuan, A. Shen, P. Wang, H. Li, J. Zhang, C. Tian, Z. Jiang, W. Li, S. Dong, A co-assembly platform engaging macrophage scavenger receptor a for lysosome-targeting protein degradation, Nat. Commun. 15 (2024) 1663.
[26] H.W. An, D.Y. Hou, J. Yang, Z.Q. Wang, M.D. Wang, R. Zheng, N.Y. Zhang, X.J. Hu, Z.J. Wang, L. Wang, D. Liu, J.F. Hao, W. Xu, Y. Zhao, H. Wang, A bispecific glycopeptide spatiotemporally regulates tumor microenvironment for inhibiting bladder cancer recurrence, Sci. Adv. 9 (2023) eabq8225.
[27] L. Zhang, D. Jing, N. Jiang, T. Rojalin, C.M. Baehr, D. Zhang, W. Xiao, Y. Wu, Z. Cong, J.J. Li, Y. Li, L. Wang, K.S. Lam, Transformable peptide nanoparticles arrest HER2 signalling and cause cancer cell death in vivo, Nat. Nanotechnol. 15 (2020) 145–153.
[28] Z. Li, S. Zhang, Y. Chen, H. Ling, L. Zhao, G. Luo, X. Wang, M.C. Hartel, H. Liu, Y. Xue, R. Haghniaz, K. Lee, W. Sun, H. Kim, J. Lee, Y. Zhao, Y. Zhao, S. Emaminejad, S. Ahadian, N. Ashammakhi, M.R. Dokmeci, Z. Jiang, A. Khademhosseini, Gelatin methacryloyl-based tactile sensors for medical wearables, Adv. Funct. Mater. 30 (2020) 2003601.
[29] J.E. Kim, J.H. Kang, W.H. Kwon, I. Lee, S.J. Park, C.H. Kim, W.J. Jeong, J.S. Choi, K. Kim, Self-assembling biomolecules for biosensor applications, Biomaterials research 27 (2023) 127.
[30] B. Wu, J. Liang, X. Yang, Y. Fang, N. Kong, D. Chen, H. Wang, A programmable Peptidic hydrogel adjuvant for personalized immunotherapy in resected stage tumors, J. Am. Chem. Soc. 146 (2024) 8585–8597.
[31] N. Kong, H. Ma, Z. Pu, F. Wan, D. Li, L. Huang, J. Lian, X. Huang, S. Ling, H. Yu, Y. Yao, De novo design and synthesis of polypeptide Immunomodulators for resetting macrophage polarization, Biodesign Research 5 (2023) 0006.
[32] H. Liang, Q. Lu, J. Yang, G. Yu, Supramolecular Biomaterials for Cancer Immunotherapy, Research (Washington, D.C.) vol. 6 (2023) 0211.
[33] H. Gao, M. Chen, Y. Liu, D. Zhang, J. Shen, N. Ni, Z. Tang, Y. Ju, X. Dai, A. Zhuang, Z. Wang, Q. Chen, X. Fan, Z. Liu, P. Gu, Injectable Anti-Inflammatory Supramolecular Nanofiber Hydrogel to Promote Anti-VEGF Therapy in Age-Related Macular Degeneration Treatment, Advanced Materials (Deerfield Beach, Fla.) 35 (2023) e2204994.
[34] X. Liu, Z. Chen, J. Bai, X. Li, X. Chen, Z. Li, H. Pan, S. Li, Q. Gao, N. Zhao, A. Chen, H. Xu, Y. Wen, L. Du, M. Yang, X. Zhou, J. Huang, Multifunctional hydrogel eye drops for synergistic treatment of ocular inflammatory disease, ACS Nano 17 (2023) 25377–25390.
[35] W. Wu, Z. Zhang, T. Xiong, W. Zhao, R. Jiang, H. Chen, X. Li, Calcium ion coordinated dexamethasone supramolecular hydrogel as therapeutic alternative for control of non-infectious uveitis, Acta Biomater. 61 (2017) 157–168.
[36] Y. Hu, Y. Wang, J. Deng, X. Ding, D. Lin, H. Shi, L. Chen, D. Lin, Y. Wang, S. Vakal, J. Wang, X. Li, Enzyme-instructed self-assembly of peptide-drug conjugates in tear fluids for ocular drug delivery, Journal of controlled release : official journal of the Controlled Release Society 344 (2022) 261–271.
[37] T. Xiong, X. Li, Y. Zhou, Q. Song, R. Zhang, L. Lei, X. Li, Glycosylation-enhanced biocompatibility of the supramolecular hydrogel of an anti-inflammatory drug for topical suppression of inflammation, Acta Biomater. 73 (2018) 275–284.
[38] K. Uesugi, H. Sakaguchi, Y. Hayashida, R. Hayashi, K. Baba, Y. Suganuma, H. Yokoi, M. Tsujikawa, K. Nishida, A self-assembling peptide gel as a vitreous substitute: a rabbit study, Invest. Ophthalmol. Vis. Sci. 58 (2017) 4068–4075.
[39] F. Danhier, E. Ansorena, J.M. Silva, R. Coco, A. Le Breton, V. Préat, PLGA-based nanoparticles: an overview of biomedical applications, Journal of controlled release : official journal of the Controlled Release Society 161 (2012) 505–522.
[40] S. Metwally, U. Stachewicz, Surface potential and charges impact on cell responses on biomaterials interfaces for medical applications, materials science & engineering, C, Materials for Biological Applications 104 (2019) 109883.
[41] H. Dong, M. Wang, S. Fan, C. Wu, C. Zhang, X. Wu, B. Xue, Y. Cao, J. Deng, D. Yuan, J. Shi, Redox-regulated conformational change of disulfide-rich assembling peptides, Angew. Chem. Int. Ed. Eng. 61 (2022) e202212829.
[42] Y.C. Liu, H.N. Gong, Z.W. Wang, C.Q. Yuan, J.R. Lu, X.H. Yan, Treatment of superbug infection through a membrane-disruption and immune-regulation Cascade effect based on supramolecular peptide hydrogels, Adv. Funct. Mater. 33 (2023) 8.
[43] Q. Zou, R. Chang, R. Xing, C. Yuan, X. Yan, Injectable self-assembled bola-dipeptide hydrogels for sustained photodynamic prodrug delivery and enhanced tumor therapy, Journal of controlled release : official journal of the Controlled Release Society 319 (2020) 344–351.
[44] M.F. Pignataro, M.G. Herrera, V.I. Dodero, Evaluation of Peptide/Protein Self-Assembly and Aggregation by Spectroscopic Methods, Molecules (Basel, Switzerland) 25 (2020) 4854.
[45] S. Qu, Y. Tang, Z. Ning, Y. Zhou, H. Wu, Desired properties of polymeric hydrogel vitreous substitute, Biomedicine & pharmacotherapy = Biomedecine & pharmacotherapie 172 (2024) 116154.
[46] Y. Jin, Y.J. Li, S.J. Song, Y.Q. Ding, Y.C. Dong, Y. Lu, D.S. Liu, C. Zhang, DNA supramolecular hydrogel as a biocompatible artificial vitreous substitute, Adv. Mater. Interfaces 9 (2022) 2101321.
[47] J. Xu, J.J. Heys, V.H. Barocas, T.W. Randolph, Permeability and diffusion in vitreous humor: implications for drug delivery, Pharm. Res. 17 (2000) 664–669.
[48] O.A. Mahroo, Visual electrophysiology and "the potential of the potentials", Eye (Lond.) 37 (2023) 2399–2408.
[49] N. Umanets, N.V. Pasyechnikova, V.A. Naumenko, P.B. Henrich, High-frequency electric welding: a novel method for improved immediate chorioretinal adhesion in vitreoretinal surgery, Graefe's archive for clinical and experimental ophthalmology =, Albrecht von Graefes Archiv fur klinische und experimentelle Ophthalmologie 252 (2014) 1697–1703.
[50] Y. Hong, T.V. Chirila, S. Vijayasekaran, W. Shen, X. Lou, P.D. Dalton, Biodegradation in vitro and retention in the rabbit eye of crosslinked poly(1-vinyl-2-pyrrolidinone) hydrogel as a vitreous substitute, J. Biomed. Mater. Res. 39 (1998) 650–659.
[51] S. Donati, S.M. Caprani, G. Airaghi, R. Vinciguerra, L. Bartalena, F. Testa, C. Mariotti, G. Porta, F. Simonelli, C. Azzolini, Vitreous substitutes: the present and the future, Biomed. Res. Int. 2014 (2014) 351804.
[52] Z. Liu, S.S. Liow, S.L. Lai, A. Alli-Shaik, G.E. Holder, B.H. Parikh, S. Krishnakumar, Z. Li, M.J. Tan, J. Gunaratne, V.A. Barathi, W. Hunziker, R. Lakshminarayanan, C. W.T. Tan, C.K. Chee, P. Zhao, G. Lingam, X.J. Loh, X. Su, Retinal-detachment repair and vitreous-like-body reformation via a thermogelling polymer endotamponade, Nat. Biomed. Eng. 3 (2019) 598–610.
[53] A. Schulz, K. Januschowski, P. Szurman, Novel vitreous substitutes: the next frontier in vitreoretinal surgery, Curr. Opin. Ophthalmol. 32 (2021) 288–293.
[54] R. Chang, C. Yuan, P. Zhou, R. Xing, X. Yan, Peptide self-assembly: from ordered to disordered, Acc. Chem. Res. 57 (2024) 289–301.
[55] R. Xing, C. Yuan, W. Fan, X. Ren, X. Yan, Biomolecular glass with amino acid and peptide nanoarchitectonics, Sci. Adv. 9 (2023) eadd8105.
[56] P. Zhou, R.R. Xing, Q. Li, J.B. Li, C.Q. Yuan, X.H. Yan, Steering phase-separated droplets to control fibrillar network evolution of supramolecular peptide hydrogels, Matter 6 (2023) 1945–1963.